J. Fluid Mech. (2007), *vol.* 582, *pp.* 203–222.
doi:10.1017/S002211200700585X Printed in the United Kingdom

Experimental study on resonantly forced interfacial waves in a stratified circular cylindrical basin

GEOFFREY W. WAKE[1], EMIL J. HOPFINGER[2] AND GREGORY N. IVEY[1]

[1]School of Environmental Systems Engineering, University of Western Australia, Crawley, Western Australia 6907, Australia

[2]LEGI, CNRS/INPG, Rue de la Piscine, BP 53, 38041, Grenoble, France

(Received 16 June 2006 and in revised form 22 January 2007)

Laboratory experiments have been performed on resonantly forced interfacial waves in a circular cylindrical basin containing a two-layer stratified fluid. The results of this shallow-water study exhibit a number of similarities to previous shallow-water studies performed in single-layer fluids, such as the generation of a large-amplitude response over a frequency bandwidth offset from the primary resonance, generation of a swirling mode at the observed resonant condition, and the significant contribution of higher harmonics. The two-layer experiments also produce results that are unique to stratified domains. In particular, the observed negative nonlinearity of the resonant condition at shallow water depth, mixing of the density interface resulting in detuning the forced response from the resonant condition, the enhanced role of viscous dissipation, and an alternative pathway for the nonlinear generation of higher-frequency waves when the layer depths are disparate. The results of this study are considered with regard to their implications for enclosed basins at the geophysical scale that are subject to near resonant forcing.

1. Introduction

The sloshing of fluid within an enclosed domain has motivated a large number of theoretical and experimental studies with application to the space industry (axisymmetric tanks) and shipping industry (rectangular tanks). Concise reviews of the work conducted during the last 40 years can be found in Faltinsen, Rognebakke & Timokha (2003) and Ibrahim (2005). Studies focus on domains for which either the horizontal length scales are comparable (three-dimensional studies) or one length scale dominates (two-dimensional studies).

Two-dimensional resonant sloshing, induced by the back-and-forth agitation of a rectangular tank filled with fluid, results in the amplification of the primary mode of the domain, with the response taking the form of a planar standing wave (e.g. Faltinsen & Timokha 2001, 2002) whose character is dependent upon the excitation amplitude A and the fluid depth h, relative to the characteristic domain length scale L (e.g. Faltinsen & Timokha 2001). As the excitation amplitude increases, the primary mode becomes large in an increased frequency bandwidth around the primary natural frequency (e.g. Faltinsen & Timokha 2001; Royon-Lebeaud, Hopfinger & Cartellier 2007). The effect of varying the aspect ratio h/L is two-fold. First, as h/L is varied,

the frequency bandwidth containing the primary mode broadens and shifts away from the natural frequency with a pronounced hysteresis (e.g. Ockendon & Ockendon 1973; Miles 1984; Faltinsen *et al.* 2000). Such behaviour is a nonlinear effect rather than due to dissipation (e.g. Miles 1984). For deep water ($h/L > 1$), this shift in the resonant condition is to forcing frequencies less than the natural frequency of the domain ($\sigma_f/\sigma_1 < 1$, σ_f is the forcing frequency and σ_1 is the natural frequency of the basin) and is referred to in the literature as negative nonlinearity (e.g. Miles 1984; Faltinsen *et al.* 2003). For shallow water ($h/L \ll 1$), this shift is to forcing frequencies greater than the natural frequency of the domain ($\sigma_f/\sigma_1 > 1$), referred to as positive nonlinearity. Secondly, for shallow water, the natural frequencies of the domain have a commensurate spectrum such that nonlinearities, introduced when the primary mode becomes large, result in secondary (internal) resonance and excitation of higher harmonics (Faltinsen & Timokha 2002; Faltinsen, Rognebakke & Timokha 2005*b*).

Three-dimensional resonant sloshing in axisymmetric (circular) and square-base cylindrical domains results in the amplification of the primary modes, with the response taking the form of either a 'planar' standing wave (in this context, the term planar refers to two-dimensional motion, e.g. Faltinsen *et al.* 2003, 2005*a*) or a rotating wave (three-dimensional motion), commonly known as a 'swirling' wave (Miles 1984; Gavrilyuk, Lukovsky & Timokha 2000). A domain with a square-based geometry introduces an additional three-dimensional wave known as a 'square' wave (Miles 1994). The frequency bandwidths where these motions are stable vary with h/L (Faltinsen *et al.* 2003, 2005*a*). In addition, there is a frequency bandwidth where no stable motions exist and chaotic motions are observed (e.g. Royon-Lebeaud *et al.* 2007); the character of the response in this domain also varies with h/L such that chaotic motions seem not to be observed for $h/L < 0.25$ (Gavrilyuk *et al.* 2000; Faltinsen *et al.* 2003, 2005*a*). The role of viscous dissipation, although observed experimentally to be generally weak in single-layer fluids (e.g. Faltinsen *et al.* 2003, 2005*a*), has been accounted for by estimating the logarithmic decrement coefficients for each natural mode and incorporating these into the numerical approach proposed by Faltinsen *et al.* (2005*a*).

The first experimental investigation into resonant sloshing of interfacial waves was undertaken by Thorpe (1968) who studied this process in a rectangular domain containing a miscible two-layer fluid. Thorpe (1968) considered deep-water $h_2/L \approx 1$ and shallow-water depths $h_2/L = 0.08$, where h_2 was the lower-layer fluid depth and L the dimension of the tank. Theories developed for single-layer fluid studies as well as the theory of Thorpe (1968) for resonantly forced interfacial waves, predict a change in nonlinear behaviour as the depth is varied; however, experiments did not show this. Mixing of the density interface owing to large-amplitude planar standing waves that were observed in the two-layer fluid at resonance was also noted. Experimental and theoretical work by La Rocca *et al.* (2002, 2005), considered an immiscible two-fluid system in a square-base tank that was subjected to roll/pitch excitation. Experiments were performed with frequencies away from the primary resonance, and swirling was not detected. However, La Rocca *et al.* (2005) quantified the role of viscous dissipation, by calculating the logarithmic decrement coefficients for the first three natural modes of the domain, as well as noting the role of secondary resonance phenomena for both free-surface and interfacial waves.

The objective of the current study is to extend the work presented above and investigate the resonant sloshing of interfacial waves in a two-layer stratified miscible fluid contained in a circular domain (i.e. a three-dimensional study) with shallow water depth, $h/L < 0.1$, where h is the equivalent depth for a two-layer fluid and $L = 2R$

the tank diameter. Of particular interest is the large-amplitude response at resonance and the question of whether a swirling wave can be generated. We aim to determine whether the results developed for application to the space and maritime industries may also assist in the understanding of the resonant response within domains at the geophysical scale, such as lakes, reservoirs and coastal embayments, that are typically characterized by shallow fluid depth ($h/L < 0.1$) and vertical density stratification (e.g. Thorpe 1974; Mysak *et al.* 1985; Antenucci & Imberger 2003).

Our approach is to perform a laboratory experiment in a circular cylindrical basin containing fluid with a two-layer stratification driven by steady periodic external forcing. We investigate the interfacial wave response over a frequency bandwidth that includes the primary mode of the basin. In particular, we focus on the influence of varying the fluid depth and the forcing amplitude, as well as investigating the role of frictional dissipation and the interfacial mixing phenomena that is expected to be observed at near-resonant forcing frequencies in this miscible two-layer stratified fluid system. The experimental facility and procedure is introduced in § 2. The results of the experimental programme are given in § 3. In § 4, the results of this study are considered in the context of previous studies on nonlinear three-dimensional sloshing, as well as the implications for enclosed basins at the geophysical scale-subject to near-resonant forcing.

2. Experimental facility and procedure

The experimental set-up is shown in figure 1. The experiments were conducted in a 98 cm diameter cylindrical Perspex tank of 50 cm depth. In a typical experiment, the tank was filled with fresh water to the desired upper-layer depth h_1, at which point a saline solution was carefully introduced beneath the lighter fresher water until the desired lower-layer depth h_2 was achieved. The amount of mixing due to the insertion of the saline solution was minimized by placing a cap over the injection point that forced the introduced denser fluid out in a radial fashion. A density profile was taken once the two-layer fluid had returned to its quiescent state, to determine the thickness of the density interface introduced by the filling process. Profiles were obtained by traversing a conductivity–temperature (CT) probe over the total depth and then using the equations of Ruddick & Shirtcliffe (1979) to compute the fluid density. In this way, the interface thickness could be measured to within 0.1 cm.

A semi-cylindrical Perspex insert (closed at the bottom), attached via a pulley system to a small d.c. motor mounted on the rotating turntable frame, was initially positioned at the free surface over one-half of the circular domain (figure 1*a*). A basin-scale forcing was modelled by oscillating the insert, using an eccentric crank and arm attached to the d.c. motor, so that over one forcing period the free surface over half of the tank was depressed by the stroke $2A$, where A is the forcing amplitude, before being restored to its mean position. Periodic forcing was achieved by repeatedly driving the insert at a constant forcing frequency σ_f, typically less than 0.07 Hz. The interface displacement created by this forcing was sampled at 2 Hz at five positions within the basin by ultrasonic interfacial wave probes (figure 1*b*), while the mid-depth upper-layer azimuthal and radial velocities near the tank centre were sampled at 5 Hz using a two-dimensional micro Acoustic Doppler Velocimeter (ADV) (figure 1*b*). Error estimates are of the order of instrument sensitivity (± 0.02 cm for the ultrasonic probes and $\pm 0.04\,\mathrm{cm\,s^{-1}}$ for the micro ADV).

The frequencies of the two primary modes in a circular domain are degenerate ($\sigma_{i,j} = \sigma_{j,i} = \sigma_i$) (e.g. Faltinsen *et al.* 2003; Royon-Lebeaud *et al.* 2007) so that herein

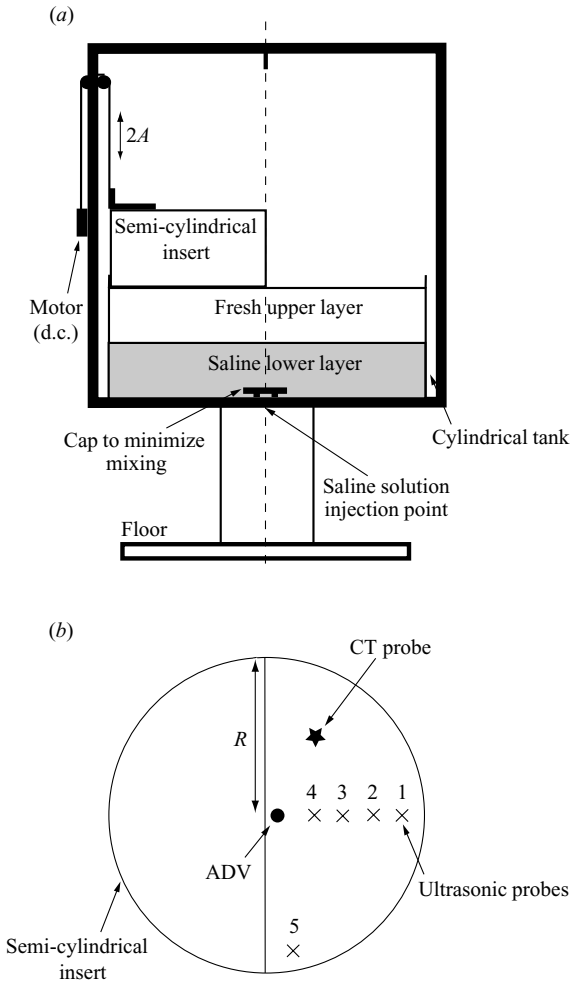

FIGURE 1. (*a*) The experimental facility. (*b*) Plan view of the circular basin indicating the location of the measurement instrumentation. The distances from the tank sidewall to probes 1–4 are 3, 13, 27 and 45 cm, respectively. Probe 5 is positioned 3 cm from the sidewall and 20 cm from the forcing mechanism. The sample volume of the micro ADV is positioned 3 cm from the tank centre.

they will be referred to simply as the *primary mode*, with a frequency σ_i. Note also that we distinguish between the lowest forced mode, or *primary forced mode*, with a frequency σ_f, and the lowest mode of the circular domain or *primary natural mode* with a frequency given by the shallow-water dispersion relation $\sigma_1 = k_1 c_0$, where $k_1 = 1.841/R$ is the horizontal wavenumber, R is the basin radius and c_0 is the linear phase speed (e.g. Lamb 1932). For a two-layer fluid, the phase speed can be approximated as $c_0 = \sqrt{g' h_E}$ where $g' = g\Delta\rho/\rho_2$ is the reduced gravity and $h_E = h_1 h_2/(h_1 + h_2)$ is the equivalent depth. Preliminary rundown experiments following a single forcing event indicated that the observed frequency of the primary natural mode was always less than the frequency calculated using the two-layer approximation for c_0 (typically with a discrepancy of about 10 %) due to the finite thickness of the interface (approximately 2 cm thick, see figure 8 for a typical density profile). To correct for this, the buoyancy frequency as a function of depth $N(z)$ was calculated from the density profile and,

Run	$2A$	h_1	h_2	h_E	g'	σ_1	σ_f/σ_1
1	0.5	19.5	19.5	9.5	10.0	0.34	<1
2	0.5	19.5	19.5	9.5	10.6	0.33	>1
3	1.0	19.5	19.5	9.5	10.0	0.33	<1
4	1.0	19.5	19.5	9.5	9.0	0.32	>1
5	1.5	19.5	19.5	9.5	9.1	0.32	<1
6	1.5	19.5	19.5	9.5	8.4	0.30	>1
7	2.0	19.5	19.5	9.5	9.1	0.32	<1
8	2.0	19.5	19.5	9.5	9.0	0.32	>1
9	1.5	13.5	13.5	6.8	11.4	0.30	<1
10	1.5	13.5	13.5	6.8	11.0	0.29	>1
11	1.5	10.0	10.0	5.0	9.2	0.24	<1
12	1.5	10.0	10.0	5.0	13.4	0.29	>1
13	1.5	7.0	20.0	5.2	11.0	0.27	<1
14	1.5	7.0	20.0	5.2	11.0	0.27	>1
15	1.5	19.5	19.5	9.5	10.1	0.33	Planar rundown
16	1.5	19.5	19.5	9.5	10.1	0.33	Swirling rundown

TABLE 1. The experimental programme: all data in c.g.s. units except for σ_1 (as determined before the start of the experiment) which is in rad s^{-1}. σ_f/σ_1 is the normalized initial forcing frequency which is not applicable for runs 15 and 16 which are rundown experiments.

following the procedure outlined in Münnich, Wüest & Imboden (1992), the true phase speed c_0 and the frequency of the primary natural mode σ_1 were determined.

In a typical experiment, periodic forcing was initiated at a prescribed frequency far from the frequency of the primary natural mode. This could be achieved in two ways, either for $\sigma_f/\sigma_1 > 1$, in which case the response of the density interface was barotropic (in phase with the free-surface displacement) or for $\sigma_f/\sigma_1 < 1$, in which case the response of the density interface was baroclinic (180° out of phase with the free-surface displacement). In the first case, for a fixed h_E and forcing amplitude A, forcing was typically initiated with a frequency in the range $\sigma_f/\sigma_1 > 1.15$. Forcing was maintained at this frequency for at least 50 forcing periods, after which time a steady-state interfacial wave response was observed (justification for the observed attainment of steady state after 50 forcing periods is presented in § 3.1.2). The forcing frequency was then decreased by a small discrete amount (by approximately $\sigma_f/\sigma_1 = 0.025$) and maintained at this new frequency for 50 forcing periods, at which point a steady-state response was again observed. This procedure of decreasing the forcing frequency by a small amount and waiting for the re-establishment of the steady-state response was repeated until $\sigma_f/\sigma_1 < 0.75$, at which point an experiment was terminated. An analogous procedure was followed for the baroclinic response (typically initiated with forcing frequency $\sigma_f/\sigma_1 < 0.75$), but in this instance the forcing frequency was repeatedly increased by small amounts until $\sigma_f/\sigma_1 > 1.15$. In this way, both approaches covered a similar frequency bandwidth of at least $0.75 < \sigma_f/\sigma_1 < 1.15$ and, for a given h_E and A, enabled us to determine whether the response exhibited a dependency upon the direction of approach to the resonant condition.

Density profiles were taken prior to each adjustment of the forcing frequency so that thickening of the density interface, owing to mixing associated with the large interface displacement at near resonant frequencies, and hence changes in c_0 and σ_1, were accounted for (see figure 8).

The experimental programme is summarized in table 1. The stroke $2A$, which was varied between 0.5 cm and 2 cm, is scaled with the basin diameter $2R$ so that the

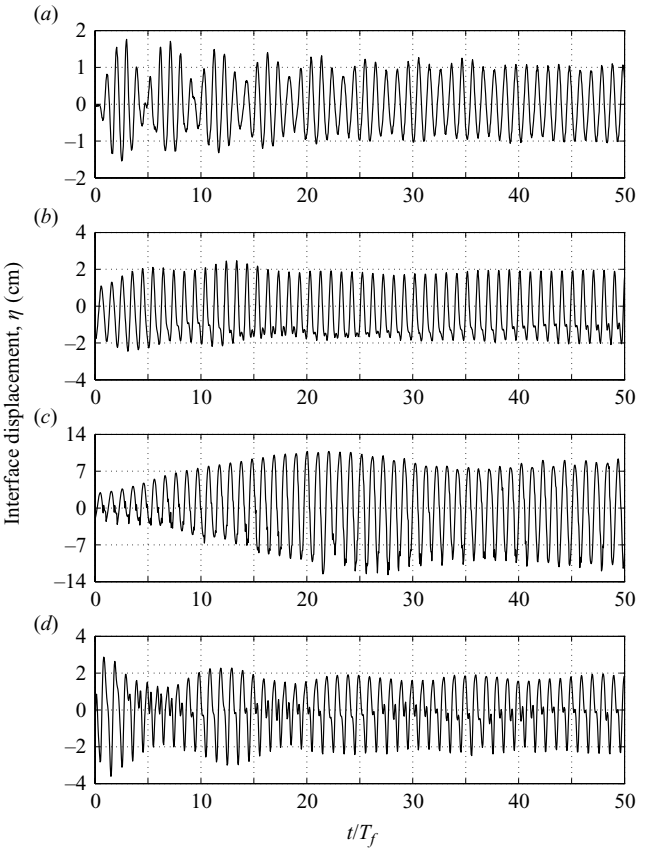

FIGURE 2. Time series of the interface displacement η of the forced response collected at 2 Hz from probe 1 for run 5 ($A/R = 0.015$, $h_E/2R = 0.1$) when (*a*) $\sigma_f/\sigma_1 = 0.76$, (*b*) $\sigma_f/\sigma_1 = 0.83$, (*c*) $\sigma_f/\sigma_1 = 0.93$, and (*d*) $\sigma_f/\sigma_1 = 1.00$. Time t has been scaled with the forcing period T_f. Interface displacement measurements are accurate to ± 0.02 cm. Note the change of vertical scale in the four plots.

dimensionless forcing amplitude A/R varied between 0.005 and 0.02. The equivalent depth h_E is also scaled with the basin diameter $2R$ with the dimensionless depth $h_E/2R$ being varied between 0.05 and 0.1, so this is a shallow-water study as $h_E/2R \ll 1$ (see Dean & Dalrymple 1992; Faltinsen & Timokha 2002).

3. Results

Interface displacement time series measured with probe 1 for a typical run (run 5) are presented in figure 2 in order to illustrate the salient features of the forced response that are ubiquitous throughout the experimental regime. The ratio of the initial forcing frequency to the frequency of the primary natural mode is $\sigma_f/\sigma_1 = 0.76$ for this run, with the interface displacement exhibiting beating owing to the interaction between the transient and forced response (figure 2*a*). After approximately 40 forcing periods, the beating phenomenon is no longer evident, probably because of the viscous dissipation of the transient response, so the time series consists of only the forced response with an interface displacement of approximately 1 cm. The forcing frequency is then increased to $\sigma_f/\sigma_1 = 0.83$, and after approximately 10 forcing periods

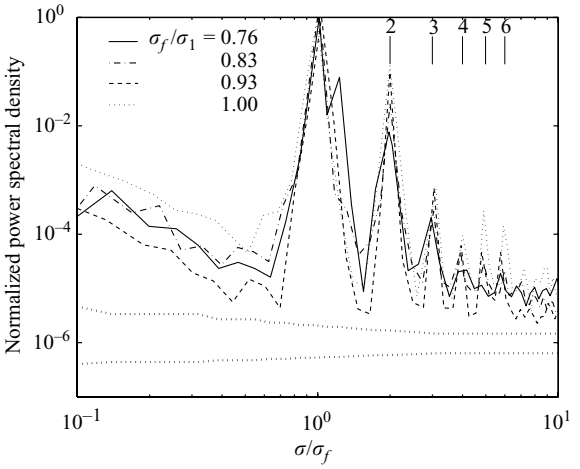

FIGURE 3. Normalized power spectra of the interface displacements η shown in figure 1. The power spectra of the interface displacement are scaled by the value noted at the observed frequency σ. The observed frequency σ is scaled by the forcing frequency σ_f. The solid vertical lines identify the frequencies of the harmonics of the primary forced mode. Spectra have been smoothed in the frequency bandwidth to improve confidence, with the 95 % confidence level shown by the dotted nearly horizontal lines.

at this new frequency, the interface displacement consists of a wave with a frequency close to the forcing frequency, and an increased amplitude of 2 cm, as well as a higher-frequency contribution that persists for the remainder of the time series record presented in figure 2(*b*). The forcing frequency is then increased again ($\sigma_f/\sigma_1 = 0.93$), resulting in the immediate and dramatic amplification of the forced response with the interface displacement increasing during the first 20 forcing periods, suggesting that near this forcing frequency resonance, and, hence excitation of the primary natural mode of the basin, is achieved (figure 2*c*). After 40 forcing periods, the interface displacement maintains a constant value of approximately 9 cm. This time series also suggests some evidence of a higher-frequency contribution (evident in the wave troughs of the forced response). An increase in forcing frequency ($\sigma_f/\sigma_1 = 1.00$) results in a dramatic reduction in the forced response amplitude as well as the now significant contribution of a higher-frequency component that persists for the entire time series record in figure 2(*d*).

Normalized power spectra of the interface displacement time series in figure 3 demonstrate the relative contribution of the wave frequencies that constitute the forced response (figure 3). In all instances, the dominant contribution of the forced response is the primary forced mode (first harmonic). When $\sigma_f/\sigma_1 = 0.76$, there is a spectral peak at a slightly higher frequency than the forcing frequency, owing to the transient response that is generated by the initial condition of the experiment, as well as evidence of contributions from the second and third harmonics. When $\sigma_f/\sigma_1 = 0.83$, there is an increased contribution by the second harmonic as well as some suggestion of minor contributions up to the fifth harmonic. The normalized power spectra for $\sigma_f/\sigma_1 = 0.93$ and $\sigma_f/\sigma_1 = 1.00$ exhibit a far greater contribution from frequencies higher than the forcing frequency. The height of the spectral peak corresponding to the second harmonic, for example, has increased significantly in comparison to that noted for $\sigma_f/\sigma_1 = 0.76$ and there are contributions up to and including the sixth harmonic. The excitation of higher interfacial harmonics near the

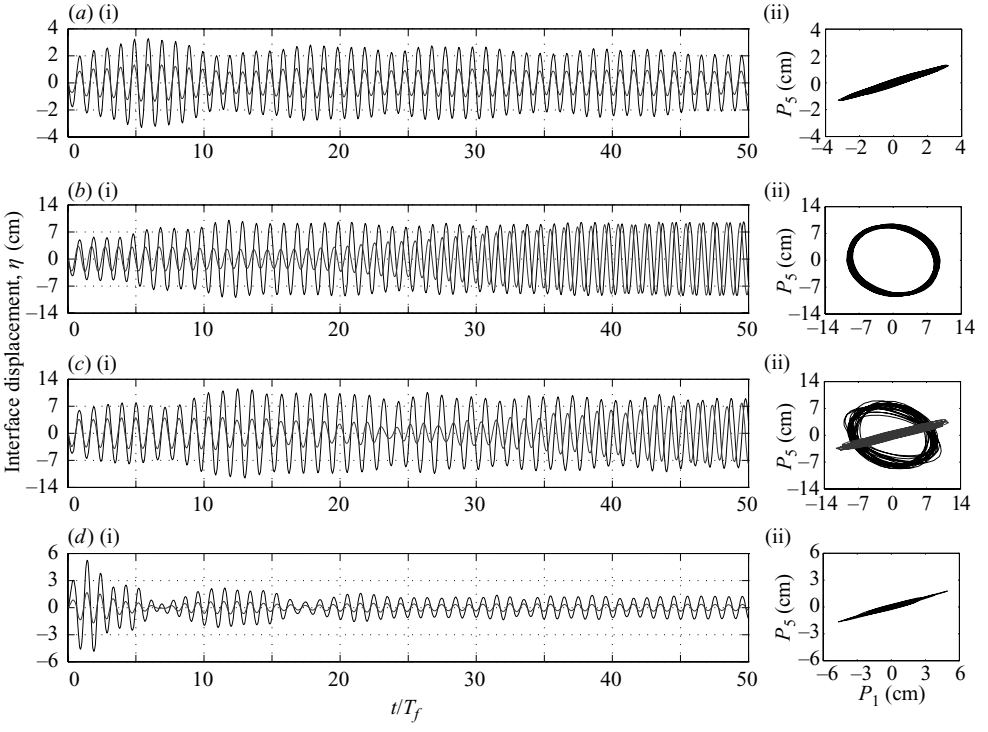

FIGURE 4. (i) Time series of the interface displacement η of the primary forced mode collected from probes 1 (solid line) and 5 (dotted line) for run 6 ($A/R = 0.015$, $h_E/2R = 0.1$) when (*a*) $\sigma_f/\sigma_1 = 1.07$, (*b*) $\sigma_f/\sigma_1 = 0.96$, (*c*) $\sigma_f/\sigma_1 = 0.92$, and (*d*) $\sigma_f/\sigma_1 = 0.78$. (ii) Interface displacement at probe 5 versus the interface displacement at probe 1 when (*a*) $\sigma_f/\sigma_1 = 1.07$, (*b*) $\sigma_f/\sigma_1 = 0.96$ (last 10 forcing periods), (*c*) $\sigma_f/\sigma_1 = 0.92$ (the first (grey) and last (black) 10 forcing periods), and (*d*) $\sigma_f/\sigma_1 = 0.78$.

resonant frequency has previously been noted experimentally and numerically in the two-layer immiscible fluid studies conducted by La Rocca *et al.* (2002, 2005) in a square domain (in particular, compare figures 2 and 3 with figure 6 in La Rocca *et al.* 2002 and figure 13 in La Rocca *et al.* 2005).

In summary, initiation of forcing results in interfacial wave beating owing to the interaction of the transient and forced response with this phenomenon decaying in time as the transient response is dissipated. As the resonant condition is approached, by small finite adjustments of the forcing frequency, amplification of the interface displacement as well as the increased contribution by higher harmonics are observed. Such behaviour is consistent with previous shallow and intermediate water studies conducted with a single- (e.g. Chester & Bones 1968; Faltinsen & Timokha 2002; Faltinsen *et al.* 2005*b*) and two-layer fluids (e.g. La Rocca *et al.* 2002, 2005). The important difference is the negative nonlinear resonance behaviour ($\sigma_f/\sigma_1 < 1$), which is different from the positive nonlinear behaviour predicted by Thorpe (1968) and in analogous single-layer-fluid studies conducted in shallow water.

3.1. *Excitation of the primary forced mode*

In order to separate the primary mode of the forced response from its higher harmonics, consider the bandpass filtered interface displacement time series of the primary forced mode for a typical run (run 6), collected at probes 1 and 5 (see figure 1), presented in figure 4. When $\sigma_f/\sigma_1 = 1.07$ (figure 4*a*(i)), the interface displacement

collected at the two locations are phase locked and the maximum interface displacement is observed at probe 1, suggesting that at this frequency, the response is a horizontal mode one planar standing wave (node at the tank centreline, see figure 1). This is further illustrated in figure 4(*a*)(ii) where the interface displacement at probe 5 versus the interface displacement at probe 1 is presented, with the observed linear relationship between the interface displacements at the two measurement locations being in agreement with the theoretical prediction for a planar standing wave (see figure 15(*c*) in Faltinsen *et al.* 2003).

This planar standing wave is maintained as the forcing frequency is decreased until $\sigma_f/\sigma_1 = 0.96$ (time series in figure 4*b*(i)). Amplification of the interface displacement is observed at probe 1 during the first 10 forcing periods at this new forcing frequency, suggesting establishment of the resonant condition. At this point, instability of the planar standing wave is visually observed across the density interface. Mixing of the density interface by this instability continues and, after a further 5–10 forcing periods, the planar standing wave begins to lose its two-dimensional character so that the two signals are no longer phase locked after 20 forcing periods. During the next 20 forcing periods, the interface displacement at probe 5 continues to increase until it is approximately equal to that measured at probe 1. The interface displacement at probe 5 versus probe 1 after 40 forcing periods is presented in figure 4(*b*)(ii), and indicates an elliptical relationship between the interface displacements measured at the two locations. An elliptical relationship has previously been shown to characterize a swirling wave (see figure 16 in Faltinsen *et al.* 2003). Experiments in a cylindrical tank with a single-layer fluid exhibited similar behaviour, with a clear transition from a planar wave to a swirling wave motion at a certain frequency and wave amplitude depending on the excitation amplitude (Royon-Lebeaud *et al.* 2007).

The swirling wave displays little interfacial mixing; however, mixing associated with planar wave instability results in sufficient thickening of the interface (after approximately 100 forcing periods) that it increases σ_1 and hence the system is detuned from the resonant condition, resulting in a reduction in interface amplitude and a return to a planar waveform. A further increase in the forcing frequency may offset the increase in σ_1 associated with the thickening of the interface so that resonance and, hence, a swirling wave may be re-established. This process is illustrated in figure 4(*c*)(i) ($\sigma_f/\sigma_1 = 0.92$) where it is evident that, while there is an amplification of the interface displacement at probe 1 during the first 15 forcing periods, the response is a planar standing wave (figure 4(*c*)(i), (ii)). After 25 forcing periods, the time series at the two measurement locations are no longer in phase and amplification at probe 5 is noted until, after approximately 45 forcing periods, the swirling wave is observed (figure 4*c*(i), (ii)). Subsequent increases in the forcing frequency result in a swirling wave being re-established (for at least 100 forcing periods) until the resonant condition is lost, at which point the interface displacement reduces dramatically and the primary mode response consists of only a planar standing wave (see figure 4*d*(i), (ii) for which $\sigma_f/\sigma_1 = 0.78$).

The behaviour of the primary forced mode over the experimental regime considered here, using a shallow two-layer fluid, follows that demonstrated previously in a single-layer fluid of intermediate depth consisting of a rotating 'swirling' wave within a frequency bandwidth around the resonant condition, whilst outside this bandwidth it is found to be a planar standing wave (e.g. Gavrilyuk *et al.* 2000; Faltinsen *et al.* 2003, 2005*b*; Royon-Lebeaud *et al.* 2007). Unlike swirling surface waves, swirling interfacial waves occur for frequencies $\sigma_f/\sigma_1 < 1$.

The influence of varying the forcing amplitude for a constant layer depth ratio ($h_E/2R = 0.1$), as depicted in figure 5 where the normalized maximum interface

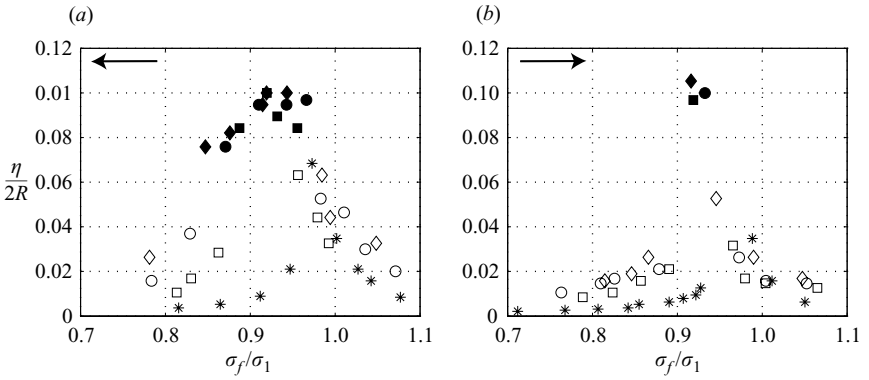

FIGURE 5. The influence of forcing amplitude A on the steady-state interface displacement η of the primary forced mode measured over a frequency bandwidth $0.7 < \sigma_f/\sigma_1 < 1.1$ at probe 1 for $h_E/2R = 0.1$. (*a*) Resonance is approached by decreasing the forcing frequency for runs 2 ($A/R = 0.005$, stars), 4 ($A/R = 0.01$, squares), 6 ($A/R = 0.015$, circles), and 8 ($A/R = 0.02$, diamonds). (*b*) Resonance is approached by increasing the forcing frequency for runs 1 ($A/R = 0.005$, stars), 3 ($A/R = 0.01$, squares), 5 ($A/R = 0.015$, circles), and 7 ($A/R = 0.02$, diamonds). The solid symbols indicate when the steady-state primary forced mode is a swirling wave.

displacement ($\eta/2R$, taken as the interface displacement after approximately 45–50 forcing periods) of the primary forced mode is plotted as a function of the normalized forcing frequency (σ_f/σ_1). In figure 5(*a*), the resonant condition is approached by decreasing the forcing frequency, whereas in figure 5(*b*), it is approached by increasing the forcing frequency. Note that the bandwidth over which resonance occurs is substantially larger in figure 5(*a*) than in figure 5(*b*). The maximum interface displacement in both is approximately $\eta/2R = 0.1$, regardless of the forcing amplitude, with this maximum occurring at a frequency of approximately $\sigma_f/\sigma_1 = 0.93$. This hysteresis and shift of the resonant condition from $\sigma_f/\sigma_1 = 1$ is due to nonlinearity, which is negative in stratified systems as opposed to positive nonlinearity observed for single layer-shallow-fluid studies (e.g. Ockendon & Ockendon 1973; Faltinsen *et al.* 2000). Nevertheless, in both figures 5(*a*) and 5(*b*), the frequency bandwidth over which resonance occurs increases noticeably as the forcing amplitude increases, a result noted in previous studies in shallow and deep water conducted with a single-layer fluid (e.g. Faltinsen & Timokha 2001; Faltinsen *et al.* 2003, 2005*a*; Royon-Lebeaud *et al.* 2007).

The bending of the frequency response curve for $\sigma_f/\sigma_1 < 1$ occurs in an analogous fashion to that of a softening spring (e.g. Hayfeh & Mook 1979), with the wave motion bifurcating to a stable swirling mode that exhibits negative nonlinearity. Specifically, when the frequency is increased by small increments, planar waves bifurcate to a swirling mode at a certain value of σ_f/σ_1 and a jump in wave amplitude occurs (figure 5*b*). Then, as the frequency is further increased, the wave amplitude decreases (soft spring behaviour) and a bifurcation to planar waves takes place. When resonance is approached by decreasing the forcing frequency by small decrements (figure 5*a*), the inverse behaviour is observed, but the values of σ_f/σ_1 at the bifurcation points are not the same. As seen in figure 5, these bifurcation points depend upon the forcing amplitude. Previous single-layer-fluid studies have demonstrated that these bifurcation points also depend upon the severity of the hysteresis which, in turn, is a function of the fluid depth h/L (e.g. Faltinsen & Timokha 2001; Faltinsen *et al.* 2003, 2005*a*). In order to illustrate the bifurcations and the hysteresis more clearly, we combine

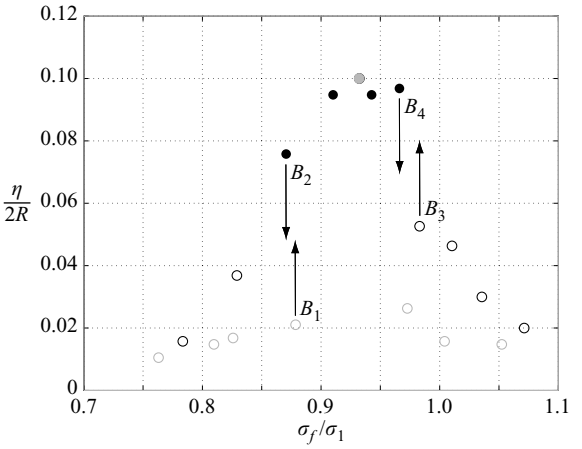

FIGURE 6. Bifurcations from planar to swirling waves and vice versa for $h_E/2R = 0.1$ and $A/R = 0.01$, illustrating the hysteresis. Results are presented for runs 3 (increasing the forcing frequency, grey circles) and 8 (decreasing the forcing frequency, black circles). The bifurcation points are labelled and the filled symbols indicate when the steady state primary forced mode is a swirling wave.

the data obtained by increasing and decreasing the forcing frequency for one forcing amplitude ($A/R = 0.01$) (figure 6). The bifurcation points are denoted by B_i with $i = 1$, 2, 3, 4. The experimental values are $B_1 \approx 0.88\sigma_f/\sigma_1$, $B_2 \approx 0.87\sigma_f/\sigma_1$, $B_3 \approx 0.98\sigma_f/\sigma_1$ and $B_4 \approx 0.96\sigma_f/\sigma_1$. The uncertainty in the values of the bifurcation points, especially in the inverse bifurcations, is due to the relatively large perturbations caused by the observed interfacial instability as well as nonlinear interactions with higher harmonics. It should also be noted that for lower forcing amplitudes ($A/R = 0.005$), the amplitude response curve does not exhibit any bifurcations because of the relatively large dissipation.

Now consider the influence of varying the fluid depth, illustrated in figure 7 in which the resonant condition is approached by decreasing the forcing frequency. Note that while it is possible to keep the depth of the thickest layer constant and vary the effective depth h_E, it is not possible to keep the effective depth constant while varying the depth of the thickest layer. In figure 7(*a–c*), the equivalent depth h_E is decreased by reducing the depth of each layer equally. As the layer depths are reduced, the frequency bandwidth over which a large-amplitude response ($\eta/2R > 0.03$) is observed increases and is shifted further from the primary natural frequency ($\sigma_f/\sigma_1 = 1$) (e.g. Ockendon & Ockendon 1973; Dean & Dalrymple 1992; Faltinsen *et al.* 2000). Now consider figure 7(*d*) in which the equivalent depth is the same as in figure 7(*c*), but the fluid depths h_1 and h_2 are not equal. Note that while the frequency bandwidth over which a large-amplitude response is observed and the maximum normalized interface displacement of the swirling wave is the same in figure 7(*c*) and figure 7(*d*), the frequency shift from the primary natural frequency is not as pronounced in figure 7(*d*) and is more akin to that noted in figure 7(*a*). The influence of the vertical length scales in two-layer stratified systems is now clear: the equivalent depth influences the extent of the frequency bandwidth around the resonant condition, while the deeper of the two fluid layers (h_2 in the example given in figure 7) determines the magnitude of the negative nonlinear shift of the resonant condition from the primary natural frequency.

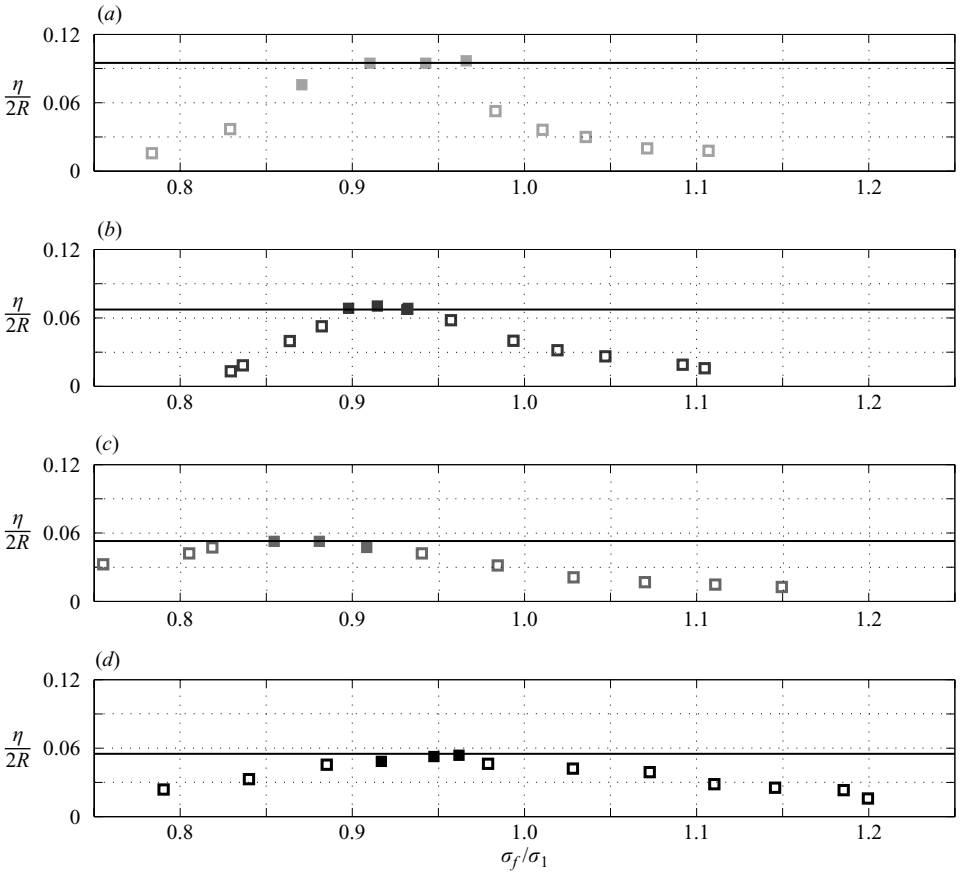

FIGURE 7. The influence of the equivalent depth h_E on the steady-state interface displacement η of the primary forced mode measured over a frequency bandwidth $0.75 < \sigma_f/\sigma_1 < 1.2$ at probe 1 for $A/R = 0.015$ (*a*) run 6 ($h_E/2R = 0.1$, $h_1 = h_2 = 19.5$ cm), (*b*) run 10 ($h_E/2R = 0.07$, $h_1 = h_2 = 13.5$ cm), (*c*) run 12 ($h_E/2R = 0.05$, $h_1 = h_2 = 10$ cm), and (*d*) run 14 ($h_E/2R = 0.05$, $h_1 = 7$ cm, $h_2 = 20$ cm). The solid horizontal line in (*a*)–(*d*) indicates the normalized equivalent depth $h_E/2R$ for each run of the experiment. The filled squares indicate when the steady-state primary forced mode is a swirling wave.

3.1.1. *Interfacial mixing*

The thickening of the density interface owing to the interfacial mixing generated by planar wave instability is reasonably pronounced, as illustrated in figure 8 in which the density profile before the commencement and after the termination of run 5 is shown (after approximately 500 forcing periods), and is sufficient to increase σ_1 such that the swirling wave is detuned from the resonant condition. In this way, mixing of the density interface places an upper bound on the wave amplitude and duration of a resonant response in stratified fluids.

Thorpe (1978), Holyer (1979) and others have argued that interfacial wave breaking in a layered stratification may occur owing to convective instability, with the convective breaking criterion being $U/c_0 \sim 1$ where U is the wave-induced velocity. Laboratory experiments by Grue *et al.* (2000) demonstrated that interfacial wave breaking due to convective instability in a two-layer fluid may still occur even when $U/c_0 \sim 0.8$. For run 5 of these experiments, the linear phase speed determined from

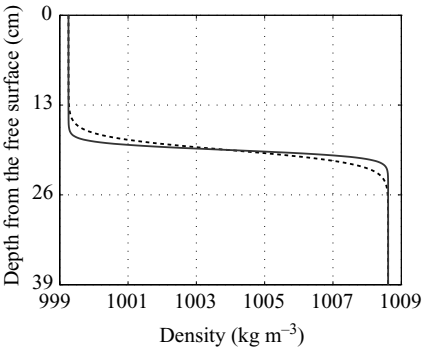

FIGURE 8. Density profiles measured with the CT probe before (solid line) and after (dashed line) run 5 of the experiment was conducted ($A/R = 0.015$, $h_E/2R = 0.1$).

figure 8 was $c_0 = 8.5\,\mathrm{cm\,s^{-1}}$ whilst the maximum observed velocity measured near the tank centre by the ADV, when interfacial instabilities are noted, was $U = 4.5\,\mathrm{cm\,s^{-1}}$ so that $U/c_0 = 0.53$. Similar values of U/c_0 are returned over the entire experimental regime suggesting that the observed interfacial instabilities are unlikely to be caused by convective instability.

The oscillatory shear flow considered here implies that using the gradient Richardson number criterion of $Ri < 0.25$ to determine whether the observed instabilities are generated by Kelvin–Helmholtz instability is not applicable (e.g. Horn, Imberger & Ivey 2001; Troy & Koseff 2005). An experimental study by Troy & Koseff (2005) on the instability of long interfacial waves showed that a reasonable Kelvin–Helmholtz instability criterion is approximately

$$Ri_w \equiv \frac{N^2(z)}{|\partial U/\partial z|^2} < 0.07 \tag{3.1}$$

where, $N(z) = \sqrt{(-g/\rho)(\mathrm{d}\rho/\mathrm{d}z)}$ is the local buoyancy frequency and $\partial U/\partial z$ is the vertical shear of the wave-induced horizontal velocity. For equal layer fluid depth, the velocity on each side of the interface can be obtained by noting that $U = \eta\sigma$ whereas the thickness of the oscillating shear layer is determined by viscosity and thus is given by $\delta_s = 5(\nu/\sigma)^{1/2}$ (Lighthill 1978, p. 131) so that (3.1) becomes

$$Ri_w \equiv \frac{N^2(z)}{(\eta\sigma)^2}(\nu/\sigma) < 0.011. \tag{3.2}$$

For run 5, for example, the maximum buoyancy frequency is $N = 2.1\,\mathrm{rad\,s^{-1}}$ (calculated from figure 8) while $\sigma = \sigma_1 = 0.32\,\mathrm{rad\,s^{-1}}$ (at resonance), so from (3.2) we expect the onset of instabilities when $\eta \geqslant 11\,\mathrm{cm}$. In the experimental study by Thorpe (1968), the buoyancy frequency was approximately $N = 1.74\,\mathrm{rad\,s^{-1}}$ while $\sigma_1 = 0.62\,\mathrm{rad\,s^{-1}}$ so that the criterion becomes $\eta \geqslant 3.4\,\mathrm{cm}$. Instability of the density interface in the present study and in Thorpe (1968) was noted after 10 and 4 cm, respectively (see figure 13 in Thorpe 1968) so that (3.2) provides a quantitative measure for predicting the onset of Kelvin–Helmholtz instabilities for basin-scale interfacial modes in both circular cylindrical (present study) and rectangular (Thorpe 1968) domains.

3.1.2. *Viscous dissipation*

Following the initiation of an experiment, there is little evidence of the transient response after approximately 40–50 forcing periods. In order to investigate this

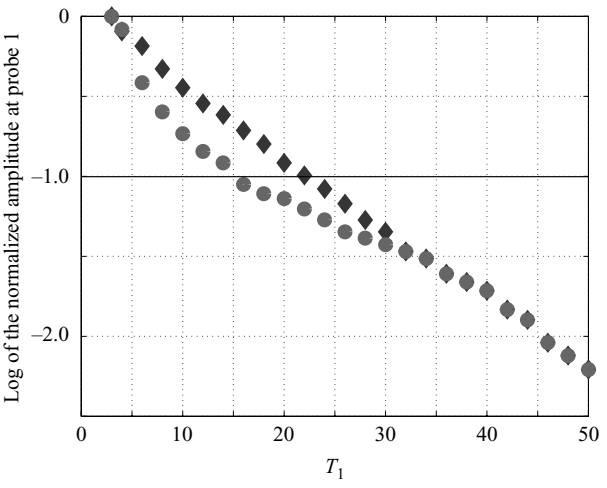

FIGURE 9. The decay of normalized interface displacement η of the primary natural mode of the basin, measured at probe 1 for rundown experiments 15 and 16. The diamonds represent the interface displacement of every second wave crest for the decaying planar wave observed in run 15. The circles represent the interface displacement of every second wave crest for the decaying swirling wave observed in run 16. The solid horizontal line indicates the point at which the normalized interface displacement is $1/e$ of its initial value.

observation further, an experiment was conducted (run 15) for which the forcing frequency was kept constant, but far from the resonant frequency of the primary natural mode, for 100 forcing periods (in order to ensure that the transient response has dissipated completely), the forcing was then stopped and the decay of the transient planar wave recorded at probe 1. Such an approach was used in the two-layer immiscible fluid laboratory studies of La Rocca *et al.* (2002, 2005) conducted in a square domain, in which it was demonstrated that the transient interfacial planar wave generated in this manner decays in an exponential fashion, owing to viscous effects.

Figure 9 illustrates the decay of the primary mode following the cessation of forcing for run 15. There is a slight frequency adjustment of the primary mode within approximately one wave period of turning off the forcing, associated with the transition from a forced to a transient response. The subsequent decay of the transient planar wave from this point, given in figure 9, is largely exponential in character, decaying slightly faster during the first $10T_1$ (T_1 being the period of primary natural mode of the domain) in comparison with the decay rate after $40T_1$. From figure 9, an estimate of the e-folding time scale is approximately $22T_1$. The amplitude of the transient response is 10 % of its initial value after 50 periods, so that our assumption that the forced response approaches a steady state after approximately 40–50 forcing periods is reasonable.

The decay is exponential of the form

$$\frac{\eta}{\eta_0} = \exp(-\kappa_1 t), \tag{3.3}$$

where $\kappa_1 = \gamma_1 \sigma_1$ for the primary natural mode of the basin. In general, dissipation on the sidewalls owing to viscous action can be written as

$$\gamma_{1s} = \frac{C}{R}(\nu/2\sigma_1)^{1/2}. \tag{3.4}$$

For deep water in a circular basin, $\sigma_1 = \sqrt{g'k_1}$, $k_1 = 1.841/R$, which gives

$$\gamma_{1s} = CR^{-3/4}\nu^{1/2}g^{-1/4}, \tag{3.5}$$

with the constant C being determined experimentally as having a value of approximately 1 (see Royon-Lebeaud *et al.* 2007). Simply replacing g by g' in (3.5) gives a predicted e-folding time scale for run 15 of approximately $50T_1$, rather than the $22T_1$ determined experimentally, suggesting that interfacial and bottom boundary dissipation are both important contributors to decay of the primary mode. For shallow water, $\sigma_1 = \sqrt{g'k_1^2 h_E}$, so that (3.4) becomes

$$\gamma_{1s} = C\left(\frac{R}{h_E}\right)^{1/4}(\nu)^{1/2}R^{-3/4}g'^{-1/4}. \tag{3.6}$$

Dissipation at the interface and the bottom is given by

$$\gamma_{1i} = \frac{C_2}{h}(\nu/2\sigma_1)^{1/2}, \tag{3.7}$$

where h is the characteristic depth (Lighthill 1978) which we take as the equivalent layer depth, so that (3.7) becomes

$$\gamma_{1i} = C\left(\frac{R}{h_E}\right)^{1/4}(\nu)^{1/2}R^{-3/4}g'^{-1/4}C_3\frac{R}{h_E}. \tag{3.8}$$

Thus, the expression for the logarithmic decrement coefficient of the primary natural mode, γ_1, in a two-layer shallow fluid with both sidewall and interfacial dissipation is given by

$$\gamma_1 = \gamma_{1s} + \gamma_{1i} = C\left(\frac{R}{h_E}\right)^{1/4}(\nu)^{1/2}R^{-3/4}g'^{-1/4}\left[1 + C_3\frac{R}{h_E}\right]. \tag{3.9}$$

The value of κ_1 and, hence, γ_1 may be determined from figure 9 which, in turn, allows us to calculate C_3 from (3.9) after assuming a value of $C \approx 1$ from single-layer theory. For run 15 of the experiment this gives $C_3 \approx 6.5$, indicating that interfacial and bottom boundary dissipation dominates wave decay in baroclinic shallow-water studies. Furthermore, the logarithmic decrement coefficient of the primary natural mode determined in this fashion is $\gamma_1 = 0.047$, which is in reasonable agreement with the value of $\gamma_1 = 0.040$ determined experimentally in the two-layer immiscible fluid study conducted by La Rocca *et al.* (2002) in a square domain.

Note that if the same experiment had been conducted in the facility with a single-layer fluid of identical total depth, then from (3.5), the e-folding time scale for the standing wave at the free surface is approximately $170T_1$. This result implies that viscous dissipation in a single-layer fluid is weak and it takes a long time for the transient response to decay, as observed in laboratory experiments performed in square-bases and circular tanks containing a single-layer fluid (e.g. Faltinsen *et al.* 2003, 2005*b*; Royon-Lebeaud *et al.* 2007).

Also presented in figure 9 is run 16, for which a swirling wave is established. During the first 10 periods following the cessation of forcing, the decay of the transient swirling wave amplitude occurred significantly faster than the exponential rate observed for the transient planar wave in run 15. This may be because during this period there is an additional pathway by which energy may be lost from the primary (swirling) mode. Specifically, this is due to the nonlinear energy transfer from the primary (swirling) mode to higher modes that occurs when the

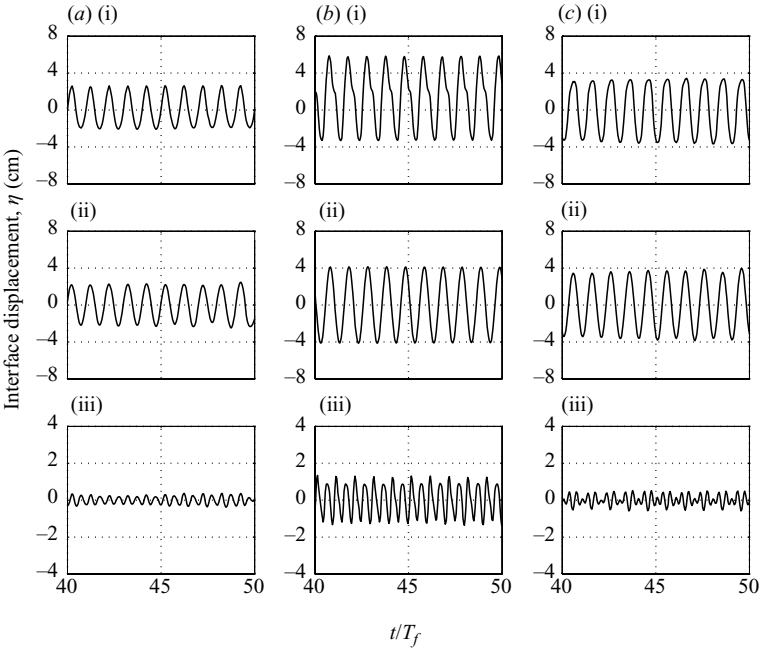

FIGURE 10. Interface displacement η of the forced response collected at probe 1 for run 9. (i) The raw time series, (ii) the time series in (i) after bandpass filtering to isolate the primary forced mode, (iii) the time series in (i) after bandpass filtering to isolate the higher-frequency components of the forced response for (*a*) $\sigma_f/\sigma_1 = 1.08$, (*b*) $\sigma_f/\sigma_1 = 0.99$, and (*c*) $\sigma_f/\sigma_1 = 0.86$.

wave amplitude is large owing to secondary (internal) resonance (this process is discussed further in § 3.2) (e.g. Faltinsen *et al.* 2005*b*; La Rocca *et al.* 2005). After some time, the primary natural mode will have decayed sufficiently that this additional pathway is no longer in operation. From figure 9, this appears to occur after 10 periods, after which time a transition from a (three-dimensional) swirling wave to a (two-dimensional) planar wave is noted, by visual inspection of the interface displacement. After approximately 30 periods, this transition is complete with the subsequent decay of the primary natural mode being exponential in character and is described well by the logarithmic decrement coefficient, γ_1, noted for run 15.

3.2. *Excitation of the higher harmonics*

The manner in which the higher harmonics may contribute to the response is illustrated in figure 10. The interface displacement measured at probe 1 is presented at three forcing frequencies (figure 10) for run 9 of the experiment. Panel (i) for each forcing frequency is the raw time series, panel (ii) is the bandpass-filtered signal corresponding to the primary forced mode, and panel (iii) is the bandpass filtered signal corresponding to the higher harmonics of the forced response. As the primary natural frequency ($\sigma_f/\sigma_1 = 1$) is approached, the amplitude of the higher harmonics increases with this contribution being as high as 20 % of the total interface displacement. As noted earlier, previous workers have suggested that the significant contribution of higher harmonics in shallow water is the result of the natural frequencies of a square or rectangular domain having a commensurate spectrum such that nonlinearities,

introduced when the primary mode becomes large, result in secondary (internal) resonance and excitation of these higher harmonics (e.g. Faltinsen & Timokha 2002; Faltinsen *et al.* 2005*b*; La Rocca *et al.* 2005). An anonymous reviewer noted that higher harmonics have a commensurate spectrum only for rectangular and square geometries and not for the Bessel modes of the circular domain considered in the present study. Nevertheless, Faltinsen *et al.* (2005*b*) observed that even if the spectrum is not commensurate, the probability of secondary resonance grows with increasing wave amplitude and thus, at near-resonant conditions, this phenomenon may still occur. To determine unequivocally whether the higher harmonics observed at near-resonant forcing are in fact higher modes generated by secondary resonance, the experimentally measured modal structure (which can be inferred from suitably bandpass-filtered interface displacement time series recorded at the 5 locations within the circular domain see figure 1) must be compared to the theoretical modal structure of the higher mode under investigation. Such an approach has been performed successfully by Wake, Ivey & Imberger (2005) and La Rocca *et al.* (2005), but goes beyond the scope of the current work.

Adopting a similar approach to that presented in figure 10, the contribution by the higher harmonics may be investigated for the entire experimental regime. For the range of forcing amplitudes considered in this study, there is little evidence of a greater contribution by higher harmonics as the forcing amplitude increases. As the equivalent depth is reduced from $h_E/2R = 0.1 - 0.05$ (by reducing the depth of each layer equally) there is evidence of increased higher harmonic activity, with the maximum contribution increasing to approximately 25 % of the amplitude of the forced response. The greatest high-frequency wave activity is observed near resonance when the equivalent depth is $h_E/2R = 0.05$ but the fluid depths h_1 and h_2 are not equal. In this instance, the contribution of waves with a frequency greater than the primary mode contribute approximately 45 % of the response. In varying the layer depths we have allowed a second mechansim that may generate high-frequency waves. Specifically, the unequal layer depths facilitate the generation of both a planar standing wave and a nonlinear progressive surge following a basin-scale forcing (e.g. Boegman, Ivey & Imberger 2005). The nonlinear surge, which has a frequency twice that of the primary forced mode, continues to steepen until such time as dispersive effects become significant and higher-frequency nonlinear waves are observed (e.g. Boegman *et al.* 2005).

This process has previously been described in laboratory studies as well as in the field (e.g. Thorpe 1971; Horn *et al.* 2001; Boegman *et al.* 2005). Evidence of this generation mechanism is provided in figure 11 which presents normalized power spectra of the interface displacement measured at probe 1 for run 5 ($h_E/2R = 0.1, h_1 = h_2$), run 11 ($h_E/2R = 0.05, h_1 = h_2$), and run 13 ($h_E/2R = 0.05, h_1 \neq h_2$) at resonance. Note that there is little difference between the power spectra for runs 5 and 11, however, for run 13 with unequal layer depths, there is a noticeable increase in the size of the spectral peak at twice the resonant frequency (owing to the nonlinear surge) as well as an increase in spectral energy over a higher-frequency bandwidth (between $\sigma/\sigma_f = 3$ and $\sigma/\sigma_f = 9$ in figure 11), which is the characteristic power spectral representation of nonlinear waves (as noted in figure 5 by Boegman *et al.* 2005).

4. Conclusions and further discussions

The results of this laboratory study conducted in shallow water ($h_E/2R \leqslant 0.1$) with a two-layer fluid, exhibit a number of similarities with previous shallow-water

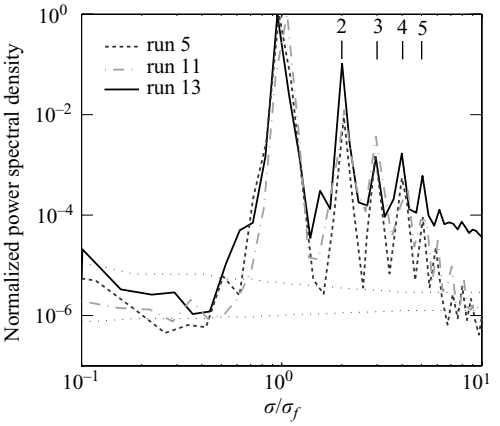

FIGURE 11. Normalized power spectra of the interface displacements η collected at probe 1 for run 5 ($A/R = 0.015$, $h_E/2R = 0.1$, $h_1 = h_2 = 19.5$ cm), run 11 ($A/R = 0.015$, $h_E/2R = 0.05$, $h_1 = h_2 = 10$ cm), and run 13 ($A/R = 0.015$, $h_E/2R = 0.05$, $h_1 = 7$ cm, $h_2 = 20$ cm) at resonance. The observed frequency σ is scaled by the forcing frequency σ_f. The solid vertical lines identify the frequencies of the harmonics of the primary forced mode. Spectra have been smoothed in the frequency bandwidth to improve confidence, with the 95 % confidence level shown by the dotted lines.

studies performed in single-layer fluids. Similarities include the generation of a large-amplitude response over a frequency bandwidth offset from the primary resonance, the generation of a swirling mode at the observed resonant condition, and the significant contribution of higher harmonics. Chaotic motions are not observed, instead planar wave motion bifurcates to a stable swirling mode and vice versa. The two-layer experiments did produce results that are unique to stratified domains. In particular, the observed negative nonlinearity of the resonant condition at shallow water depth, mixing of the density interface, by shear instabilities, resulting in the detuning of the response from the resonant condition, the enhanced role of viscous dissipation in comparison to single-layer-fluid studies, and an alternative pathway for the nonlinear generation of higher-frequency waves when layer depths are disparate.

One aspect of the single-layer-fluid studies that has yet to be discussed in the present work is what is termed 'local near-wall phenomena' which refers to the run-up of fluid up the sidewalls of the tank accompanied by splashing/overturning with possible drop formation (e.g. Faltinsen *et al.* 2003; Royon-Lebeaud *et al.* 2007). This instability of the air–water interface is pronounced at resonance, even for small forcing amplitudes, so that at some critical (large) wave displacement, additional energy provided by the resonant forcing manifests itself as local near-wall phenomena. With a two-layer fluid, such local near-wall phenomena are not permitted by the presence of the upper layer. In this instance, the maximum allowable interface displacement of the primary mode at resonance is constrained by mixing of the density interface so that interfacial wave instability may be considered to be the two-layer analogue of the 'local near-wall phenomena' and chaos noted in single-layer studies.

The present study has demonstrated that a swirling wave can be generated at near resonant forcing in shallow stratified fluids, a result with potential implications for enclosed water bodies such as lakes and reservoirs. The traditional view of fluid motion within such stratified systems is that, so long as the characteristic horizontal scale of the domain R is less than the characteristic scale at which the Earth's rotation

begins to influence fluid motion (given by the baroclinic Rossby radius of deformation $R_i = c_0/f$, where f is the Coriolis frequency), then following a uni-directional periodic forcing (typically by the wind) the response is believed to be predominantly two-dimensional (e.g. Mortimer 1974; Imberger 1998). The findings of this study suggest that three-dimensional motions may be possible in special circumstances if such a system were subject to periodic forcing close to the natural frequency of the domain. This, in turn, would influence the fate and transport of sediments, nutrients and other biological agents within such water bodies.

Another outcome of the current work for the study of stratified water bodies is the nonlinear excitation of higher harmonics by secondary resonance. As noted in § 3.2, significant advances have been made in recent years in the understanding of the energy transfer from the basin-scale to the smallest scales of motion within enclosed water bodies. One such pathway involves the nonlinear steepening of the basin-scale wave-resulting in the transfer of energy to nonlinear waves with a much shorter length scale (e.g. Horn *et al.* 2001; Boegman *et al.* 2005). Nonlinear internal resonance to higher harmonics from the primary mode would provide another pathway by which energy could be transferred from the basin-scale to waves with a much shorter length scale. Such small-scale motions have been shown to propagate to the boundary and break, thus directly affecting the distribution of sediments, nutrients and other biological agents, and hence influence the water quality within such a system (e.g. Boegman *et al.* 2003, 2005).

The authors are grateful to the three anonymous referees for useful comments on an initial draft of the manuscript. E. J. H. is grateful for the Gleddon Visiting Senior Fellowship that enabled his visit to the School for Environmental Systems Engineering. This research was funded by the Australian Research Council and The Centre for Sustainable Mine Lakes and forms School for Environmental Systems Engineering reference SESE 0004.

REFERENCES

Antenucci, J. P. & Imberger, J. 2003 The seasonal evolution of wind/internal wave resonance in Lake Kinneret. *Limnol. Oceanogr.* **48**, 2055–2061.

Boegman, L., Imberger, J., Ivey, G. N. & Antenucci, J. P. 2003 High-frequency waves in large stratified lakes. *Limnol. Oceanogr.* **48**, 895–919.

Boegman, L., Ivey, G. N. & Imberger, J. 2005 The energetics of large-scale internal wave degeneration in lakes. *J. Fluid Mech.* **531**, 159–180.

Chester, W. & Bones, J. A. 1968 Resonant oscillation of water waves. ii. Experiment. *Proc. R. Soc. Lond.* **306**, 23–30.

Dean, R. G. & Dalrymple, R. A. 1992 *Water Wave Mechanics for Engineers and Scientists*. World Scientific.

Faltinsen, O. M. & Timokha, A. N. 2001 An adaptive multimodal approach to nonlinear sloshing in a rectangular tank. *J. Fluid Mech.* **432**, 167–200.

Faltinsen, O. M. & Timokha, A. N. 2002 Asymptotic modal approximation of nonlinear resonant sloshing in a rectangular tank with small fluid depth. *J. Fluid Mech.* **470**, 319–357.

Faltinsen, O. M., Rognebakke, O. F., Lukovsky, I. A. & Timokha, A. N. 2000 Multidimensional modal analysis of nonlinear sloshing in a rectangular tank with finite water depth. *J. Fluid Mech.* **407**, 201–234.

Faltinsen, O. M., Rognebakke, O. F. & Timokha, A. N. 2003 Resonant three-dimensional nonlinear sloshing in a square-base basin. *J. Fluid Mech.* **487**, 1–42.

Faltinsen, O. M., Rognebakke, O. F. & Timokha, A. N. 2005*a* Classification of three-dimensional sloshing in a square-base tank with finite depth. *J. Fluids Struct.* **20**, 81–103.

Faltinsen, O. M., Rognebakke, O. F. & Timokha, A. N. 2005*b* Resonant three-dimensional nonlinear sloshing in a square-base basin. Part 2. Effect of higher modes. *J. Fluid Mech.* **523**, 199–218.

Gavrilyuk, I., Lukovsky, I. A. & Timokha, A. N. 2000 A multimodal approach to nonlinear sloshing in a circular cylindrical tank. *Hybrid Meth. Engng* **2**, 463–483.

Grue, J., Jensen, P., Rusas, P. & Sveen, J. K. 2000 Breaking and broadening of internal solitary waves. *J. Fluid Mech.* **413**, 181–217.

Hayfeh, A. H. & Mook, D. T. 1979 *Nonlinear Oscillations*. Wiley.

Holyer, J. Y. 1979 Large amplitude progressive interfacial waves. *J. Fluid Mech.* **93**, 433–448.

Horn, D. A., Imberger, J. & Ivey, G. N. 2001 The degeneration of large-scale interfacial gravity waves in lakes. *J. Fluid Mech.* **434**, 181–207.

Ibrahim, R. A. 2005 *Liquid Sloshing Dynamics*. Cambridge University Press.

Imberger, J. 1998 Flux paths in a stratified lake – a review. In *Physical Processes in Lakes and Oceans*. AGU Press.

La Rocca, M., Sciortino, G. & Boniforti, M. A. 2002 Interfacial gravity waves in a two-fluid system. *Fluid Dyn. Res.* **30**, 31–66.

La Rocca, M., Sciortino, G. & Adduce, C. 2005 Experimental and theoretical investigation on the sloshing of a two-fluid system with free surface. *Phys. Fluids* **3**, 983–994.

Lamb, H. 1932 *Hydrodynamics*. Dover.

Lighthill, J. 1978 *Waves in Fluids*. Cambridge University Press.

Münnich, M., Wüest, A. & Imboden, D. M. 1992 Observations of the second vertical mode of the internal seiche in an alpine lake. *Limnol. Oceanogr.* **37**, 1705–1719.

Miles, J. W. 1984 Resonantly forced surface waves in a circular cylinder. *J. Fluid Mech.* **149**, 15–31.

Miles, J. W. 1994 Faraday waves: rolls versus squares. *J. Fluid Mech.* **269**, 353–371.

Mortimer, C. H. 1974 Lake hydrodynamics. *Mitt. Intl Verein. Limnol.* **27**, 124–197.

Mysak, L. A., Salvadé, G., Hutter, K. & Scheiwiller, T. 1985 Topographic waves in a stratified basin with application to the lake of Lugano. *Phil. Trans. R. Soc. Lond.* A **316**, 1–55.

Ockendon, J. R. & Ockendon, H. 1973 Resonant surface waves. *J. Fluid. Mech* **59**, 397–413.

Royon-Lebeaud, A., Hopfinger, E. J. & Cartellier, A. 2007 Liquid sloshing and wave breaking in circular and square-base cylindrical containers. *J. Fluid Mech.* **577**, 467–494.

Ruddick, B. R. & Shirtcliffe, T. G. L. 1979 Data for double diffusers: physical properties of aqueous salt–sugar solutions. *Deep-Sea Res.* **26**, 775–787.

Thorpe, S. A. 1968 On standing internal gravity waves of finite amplitude. *J. Fluid Mech.* **32**, 489–528.

Thorpe, S. A. 1971 Asymmetry of the internal seiche in Loch Ness. *Nature* **231**, 306–308.

Thorpe, S. A. 1974 Near-resonant forcing in a shallow two-layer fluid: a model for the internal surge in Loch Ness? *J. Fluid Mech.* **63**, 509–527.

Thorpe, S. A. 1978 On the shape and breaking of finite amplitude internal gravity waves in a shear flow. *J. Fluid Mech.* **85**, 7–31.

Troy, C. D. & Koseff, J. R. 2005 The instability and breaking of long internal waves. *J. Fluid Mech.* **543**, 107–136.

Wake, G. W., Ivey, G. N. & Imberger, J. 2005 The temporal evolution of baroclinic basin-scale waves in a rotating circular basin. *J. Fluid Mech.* **523**, 367–392.